Clim Dyn
DOI 10.1007/s00382-012-1503-0

The rendition of the Atlantic Warm Pool in the reanalyses

Vasubandhu Misra · Ashley Stroman · Steven DiNapoli

Received: 10 April 2012 / Accepted: 18 August 2012

Abstract The Atlantic Warm Pool (AWP) region, which is comprised of the Gulf of Mexico, Caribbean Sea and parts of the northwestern tropical Atlantic Ocean, is one of the most poorly observed parts of the global oceans. This study compares three ocean reanalyses, namely the Global Ocean Data Assimilation System of National Centers for Environmental Prediction (NCEP), the Climate Forecast System Reanalysis (CFSR) of NCEP, and the Simple Ocean Data Assimilation (SODA) for its AWP variation. The surface temperature in these ocean reanalyses is also compared with that from the Extended Range SST version 3 and Optimally Interpolated SST version 2 SST analyses. In addition we also compare three atmospheric reanalyses: NCEP-NCAR (R1), NCEP-DOE (R2), and CFSR for the associated atmospheric variability with the AWP. The comparison shows that there are important differences in the climatology of the AWP and its interannual variations. There are considerable differences in the subsurface ocean manifestation of the AWP with SODA (CFSR) showing the least (largest) modulation of the subsurface ocean temperatures. The remote teleconnections with the tropical Indian Ocean are also different across the reanalyses. However, all three oceanic reanalyses consistently show the absence of any teleconnection with the eastern equatorial Pacific Ocean. The influence of the AWP on the tropospheric temperature anomalies last for up to a one season lead and it is found to be relatively weak in R1 reanalyses. A simplified SST anomaly equation initially derived for diagnosing El Niño Southern Oscillation variability is adapted for the AWP variations in this study. The analysis of this equation reveals that the main contribution of the SST variation in the AWP region is from the variability of the net heat flux. All three reanalyses consistently show that the role of the ocean advective terms, including that associated with upwelling in the AWP region, is comparatively much smaller. The covariance of the SST tendency in the AWP with the net heat flux is large, with significant contributions from the variations of the surface shortwave and longwave fluxes.

Keywords Atlantic Warm Pool · ENSO · Tropospheric temperature

V. Misra (✉) · A. Stroman
Department of Earth, Ocean and Atmospheric Science, Florida State University, Tallahassee, FL 32306, USA
e-mail: vmisra@fsu.edu

V. Misra · S. DiNapoli
Center for Ocean-Atmospheric Prediction Studies, Florida State University, Tallahassee, FL 32306, USA

V. Misra
Florida Climate Institute, Florida State University, Tallahassee, FL 32306, USA

1 Introduction

The Atlantic Warm Pool (AWP), as the name suggests, is the Atlantic component of the Western Hemisphere Warm Pool (WHWP; Wang and Enfield 2001). The WHWP extends over parts of the tropical eastern North Pacific (ENP) and into the AWP region. The area of the ENP is comparably much smaller than the AWP and, thereby, the WHWP as a whole is more influenced by the AWP (Wang et al. 2008). The AWP is a region of warm SST ($\geq$28.5 °C) that climatologically is known to extend over the Gulf of Mexico, the Caribbean Sea and the western part of the tropical Atlantic Ocean. The AWP has a very robust seasonal cycle, with the areal extent of the 28.5 °C isotherm

Published online: 01 September 2012

peaking in August–September–October (ASO) season (Wang and Enfield 2003). It has been shown from observational studies that the AWP undergoes frequency modulation on several time scales including intraseasonal (30–50 days; Maloney and Hartmann 2000; Higgins and Shi 2001), seasonal (Wang and Enfield 2003), interannual (Wang and Enfield 2001; Wang et al. 2006; Misra 2009) and decadal (Wang et al. 2008). The variability of the AWP in each of these time scales is also related to tropical cyclone activity in the Atlantic Ocean. For example, Wang and Lee (2007) suggest that the AWP serves as a conduit for the observed relationship between the Atlantic Multidecadal Oscillation (AMO) and the Atlantic hurricane activity. It is seen that the warm (cool) phases of the AMO are characterized by large (small) AWPs. Since the AWP resides in the genesis region of most Atlantic tropical cyclones, the influence of the AMO on Atlantic tropical cyclone activity may operate through the mechanism of the AWP-induced atmospheric changes. Similarly, such teleconnections of cyclone activity in the Atlantic with the AWP are established at other time scales (Wang et al. 2006). This teleconnection of the AWP with tropical cyclone activity significantly relates to the bloom of Gambierdiscus toxicus, a parasitic microalgal species that harps on disturbances and dislocation of algae in the coral reef areas (Tester et al. 2010).

On interannual time scales, the large AWPs that appear in certain years can be almost 3 times larger than small AWP occurrences (Wang et al. 2006). These anomalous AWP events affect rainfall over the Caribbean, Central America, and eastern South America. Furthermore, such large (small) AWP events are associated with a decrease (increase) in sea level pressure and an increase (decrease) in atmospheric convection and cloudiness, which corresponds to weak (strong) tropospheric vertical wind shear and a deep (shallow) warm upper ocean, thus, increasing (decreasing) Atlantic hurricane activity. Despite the large interannual variations of the AWP events, they seem to be largely disconnected from the interannual variations associated with El Niño Southern Oscillation (ENSO) in the equatorial Pacific Ocean (Wang and Enfield 2003). This is likely a result of ASO season being the seasonal peak of AWP when the influence of ENSO on the tropical Atlantic is the weakest. Enfield and Mayer (1997) showed that ENSO has a significant influence on the north tropical Atlantic SST in the boreal spring season. Wang and Enfield (2003) show that nearly two thirds of the overall AWP anomalies in the ASO season in the last few decades have occurred independent of the ENSO variability in the tropical Pacific.

Intriguingly, the AWP is one of the most poorly observed regions of the global oceans (Misra et al. 2010). Misra et al. (2010) show that the density of in situ ocean observations over the AWP region is comparable to the poorly observed polar oceans. In this context, this paper provides a perspective on the depiction of the AWP in three ocean reanalyses products, two atmospheric reanalyses, and two SST analyses. These datasets are described in the following section. A comparison of the AWP diagnostics between all these reanalyses are described in the results section, Sect. 3, followed by concluding remarks in Sect. 4.

2 Description of data

The ocean reanalyses used in this study are the National Centers for Environmental Prediction (NCEP) Global Ocean Data Assimilation (GODAS; Behringer and Xue 2004), NCEP Climate Forecast System Reanalyses (CFSR; Saha et al. 2010) and the Simple Ocean Data Assimilation, version 2.1.6 (SODA; Carton and Giese 2008). For atmospheric reanalyses we use the NCEP-National Center for Atmospheric Research (NCAR; R1; Kalnay et al. 1996), NCEP-Department of Energy (DOE) reanalyses (R2; Kanamitsu et al. 2002) and the NCEP CFSR. For the SST analyses we have used the Extended Reynolds SST version 3 (ERSSTv3; Smith et al. 2008) and Optimally Interpolated SST version 2 (OISSTv2; Reynolds et al. 2002). Each of these datasets is briefly discussed in the following subsections. We have compared all of these products for a common period of 1980–2006 with the exception that OISSTv2 is available from 1982. We have also removed the linear trend from all variables analyzed in this paper.

2.1 NCEP GODAS

The NCEP GODAS was developed using the three-dimensional variational scheme for data assimilation with the Geophysical Fluid Dynamics Modular Ocean Model version 3 (MOM3) as the data assimilation model. MOM3 in this assimilation was forced with NCEP-DOE (also called reanalysis 2; Kanamitsu et al. 2002) atmospheric fluxes. NCEP GODAS assimilates both surface and subsurface temperature observations. It utilizes NCEP's in situ SST observations and blended satellite analysis (Reynolds et al. 2002). The surface salinity is relaxed to annual salinity climatology (Conkright et al. 1999). The subsurface ocean temperature includes those from XBTs, profiling floats and TAO moorings. It also assimilates synthetic salinity profiles from local temperature and salinity profiles derived from Levitus climatology. GODAS is available on a quasi-global domain that extends from 75°S to 65°N. The ocean model has a 1° longitudinal resolution and 1° latitudinal resolution, which is then enhanced to 1° longitudinal resolution and 1/3° latitudinal resolution within 10° of the equator. This data is available from 1979 to the present.

2.2 NCEP CFSR

This is a very recently released coupled ocean–land–atmosphere reanalyses for a 31-year period from 1979 to 2009, which will be extended as an operational real time product (Saha et al. 2010). NCEP CFSR is substantially different from the previous NCEP-NCAR reanalysis (Kalnay et al. 1996) in that it uses the 6 h forecast field from an updated version of the coupled ocean–atmosphere–land model for the generation of the first guess field for the assimilation cycle of the individual components of the physical climate system (viz., ocean, land, and atmosphere), assimilates satellite radiances by Grid point Statistical Interpolation (GSI) scheme (Kleist et al. 2009) throughout the 31 year period and uses prescribed CO_2 concentrations as a function of time. Furthermore compared to the coarse horizontal and vertical resolution of T62L28 of the atmospheric analyses of NCEP-NCAR, NCEP CFSR is available at T382L64, and also includes ocean analyses at a latitudinal spacing of 0.25° at the equator, extending to a global 0.5° beyond the tropics, with 40 levels to a depth of 4,737 m. NCEP CFSR also includes land surface analyses with four soil levels and a global sea ice analyses with three layers. In CFSR the SST is nudged towards OISSTv2.

2.3 SODA

The ocean model in the SODA is based on the Los Alamos implementation of the Parallel Ocean Program version 2.1 (POP2.1; Smith et al. 1992). The model is constrained by temperature and salinity observations using a sequential assimilation algorithm following Carton et al. (2000a, b), Carton and Giese (2008), and Zheng and Giese (2009). The ocean model has 40 levels in the vertical, with 10 m resolution at the surface, and it has a grid spacing of 0.4° (longitude) × 0.25° (latitude). In addition, the Arctic Ocean is fully resolved since the pole is displaced (Carton et al. 2000a, b; Carton and Giese 2008; Zheng and Giese 2009).

The ocean model is forced with ERA-40 wind stresses for the period 1958–2001; for the period 2002–2008 it is forced by ERA-interim winds. Bulk formulae are used to calculate surface heat fluxes (Smith et al. 1992) for which the atmospheric variables are taken from NCEP-NCAR (Kalnay et al. 1996). The NCEP–NCAR reanalysis information is used for the bulk formulas instead of the ERA-40 variables to give continuity of surface forcing during periods for which the ERA-40 winds are not available

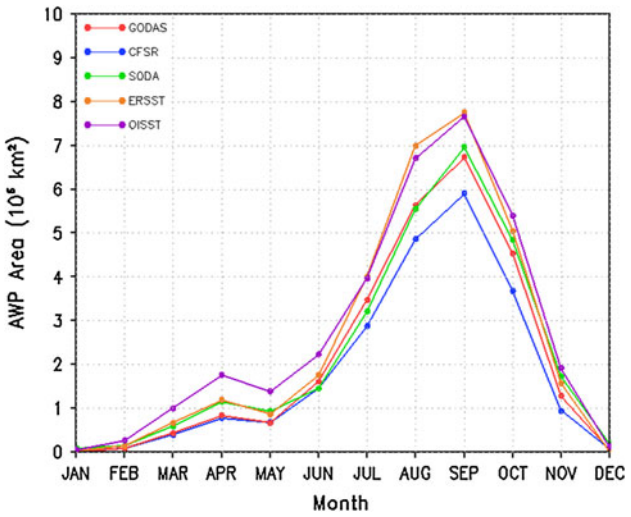

Fig. 1 Climatological monthly mean area of the AWP from ocean reanalyses and SST analyses

Table 1 The climatological area of the AWP for September from the three reanalyses and SST analysis products at their native and interpolated to common (GODAS) grid resolution

Grid	GODAS	CFSR	SODA	ERSST	OISST
Native	6.713	5.922	7.065	7.788	7.702
Interpolated	6.713	5.403	6.608	6.723	6.640

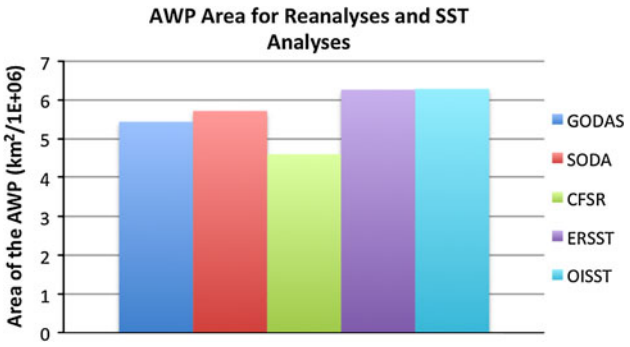

Fig. 2 The climatological area of the AWP during ASO season

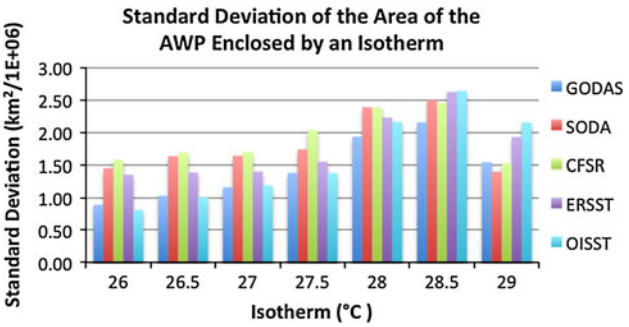

Fig. 3 The interannual variability (as shown by standard deviation) of the area enclosed by various isotherms in August–September–October (ASO) season from *top*) the three ocean reanalyses, and *bottom*) the two SST analyses. Isotherms exceeding 29.0 °C are not included to keep the sample size uniform as there were years when the SST never reached over 29 °C in the region

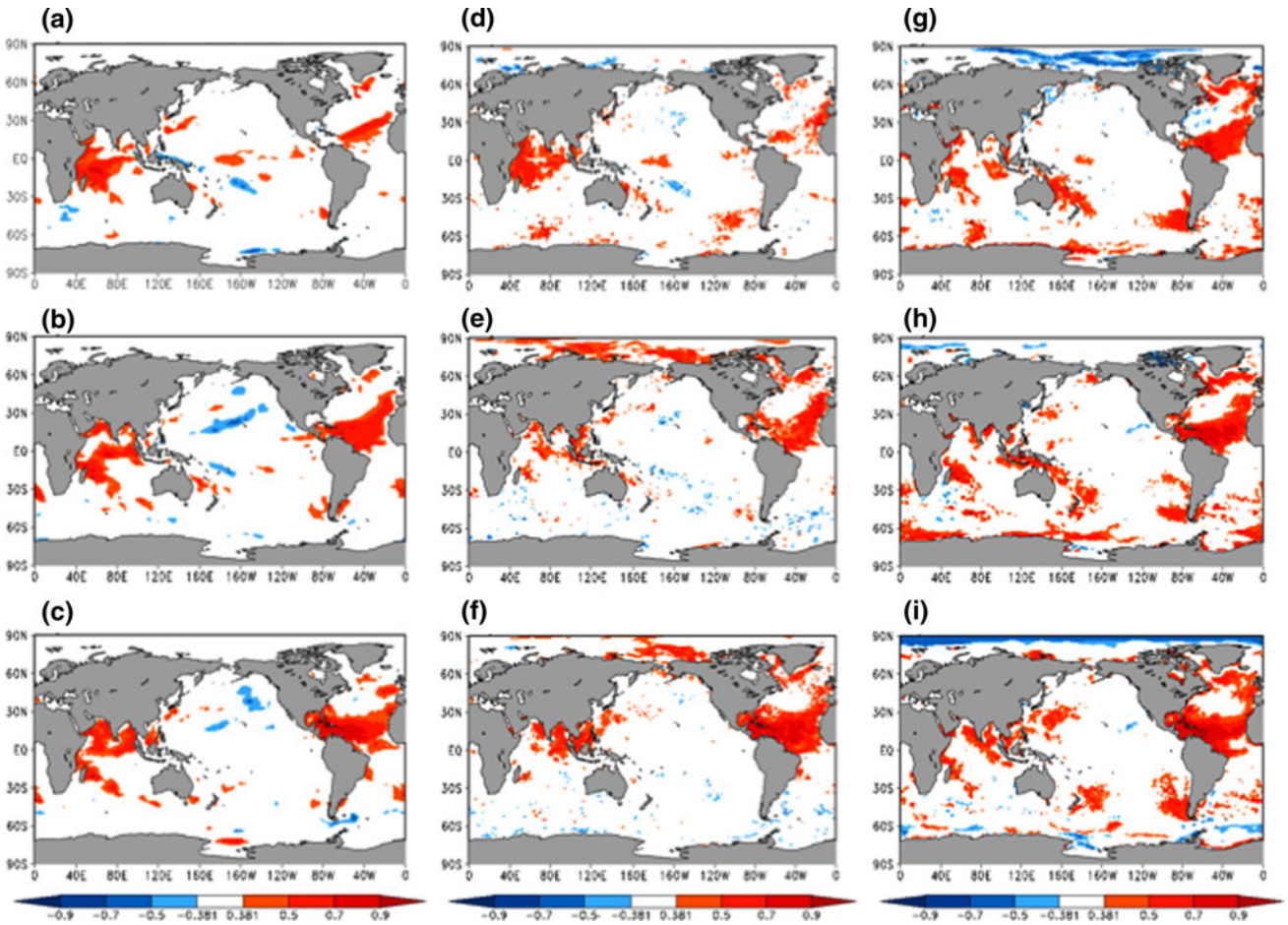

Fig. 4 The correlation of ASO averaged AWP area with **a** preceding February–March–April (FMA), **b** preceding May–June–July (MJJ), and **c** contemporaneous ASO global SSTA from GODAS. **d**, **e**, and **f** Similar to **a**, **b**, and **c** but from SODA. **g**, **h**, and **i** Similar to **a**, **b**, and **c** but from CFSR. Only statistically significant values at 95 % confidence interval according to *t* test are shown

(Zheng et al. 2010). The model output, temperature, salinity, and velocity are mapped onto a uniform 0.5° × 0.5° grid, with 40 vertical levels (Zheng and Giese 2009).

2.4 NCEP-NCAR (R1)

Upper-air and land surface data from R1 are included in this study. The data are available on a 2.5° × 2.5° grid (144 × 73) from 1948 to the present. The NCEP global spectral model (Kalnay et al. 1996) is the atmosphere model in R1. The model has a horizontal grid spacing of T62, roughly 210 km, and 28 vertical "sigma" levels. The analysis scheme used is the spectral statistical interpolation (SSI), a three-dimensional variable (3DVAR) scheme that is cast in spectral space (Parrish and Derber 1992; Derber et al. 1991). The reanalysis model uses a diagnostic cloud scheme from Campana et al. (1994) that has led to model output of outgoing longwave radiation that better matches the radiation in observations (Kalnay et al. 1996). In addition, the reanalysis model uses a two-layer land surface model (LSM) that was developed at Oregon State University by Pan and Mahrt (1987).

2.5 NCEP-DOE (R2)

This study also analyzes upper-air data from R2, which are available on a 2.5° × 2.5° grid (144 × 73) from 1979 to the present. The atmosphere model in R2 is the NCEP global spectral model (Kanamitsu et al. 2002). R2 is considered to be an updated version of R1 because human processing errors were eliminated, parameterizations of physical processes were updated, and upgrades and improvements were made to the forecast model and diagnostic package (Kanamitsu et al. 2002).

Among the improvements most pertinent to this study is smoother orography, which led to better estimations of sensible and latent heat fluxes in R2. Additionally, a new shortwave radiation scheme by Chou (1992) and Chou and Lee (1996) was used, which reduced the excessive insolation at the surface that was found in R1. Furthermore,

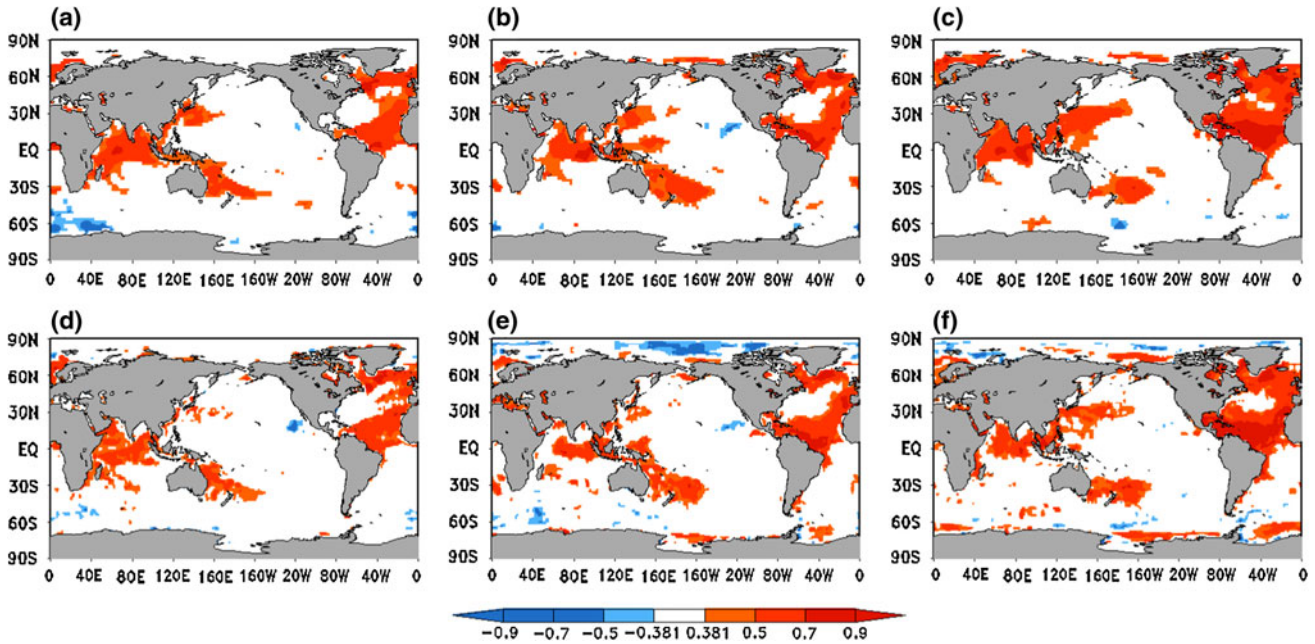

Fig. 5 The correlation of ASO averaged AWP area with **a** preceding February–March–April (FMA), **b** preceding May–June–July (MJJ), and **c** contemporaneous ASO global SSTA from ERSSTv3. **d**, **e**, and **f** similar to **a**, **b**, and **c** but from OISSTv2. Only statistically significant values at 95 % confidence interval according to *t* test are shown

minor tuning to the convective parameterization, enhancement of the longwave radiation cloud-top cooling, and updating the parameterization of stratus clouds helped in improving the simulation of the shortwave fluxes in the reanalysis. The radiation fluxes at the surface in R2 were also improved relative to R1 with corrections made to the desert albedo (Breigleb et al. 1996).

3 Results

3.1 Seasonal variation of the AWP

Figure 1 shows the seasonal cycle of the area of the AWP in the three reanalyses and two SST analyses. Although all of them show a seasonal peak in the area of the AWP in September, there is a significant underestimation of the area in September by the ocean reanalyses relative to the two SST analyses. In Table 1 (and Fig. 1) it is apparent that SODA and GODAS display nearly the same climatological area of the AWP in September but are underestimating relative to ERSST and OISST by nearly 1×10^6 km^2 whereas, CFSR seems to underestimate the area of the AWP in September by nearly 2×10^6 km^2 (Table 1). It should, however, be mentioned that these areas were calculated on the native grids of the respective reanalyses and SST analyses, which vary considerably and could potentially lead to some of these observed differences between the data products. Therefore, we recomputed the September climatological area of the AWP for all the data products used in this study by linearly interpolating to the resolution of the GODAS grid (which was chosen arbitrarily). Table 1 again shows that qualitatively the results seem consistent from our previous analysis on the native grids, with similar underestimation of the area of the AWP by the reanalyses relative to the SST analyses. Given that we will be focusing on the ASO season (the seasonal peak of the AWP) in the rest of the paper, we recomputed the climatological area of the AWP for the ASO season in Fig. 2. This figure continues to show that CFSR displays the smallest climatological area of the AWP followed by GODAS and then SODA relative to the two SST analyses, which are nearly alike.

The choice of the 28.5 °C isotherm as the critical isotherm to define the AWP by Wang and Enfield (2001) seems to also coincide with the fact that the area enclosed by it in the ASO season in the Atlantic Ocean displays the most interannual variability than any other isotherm (Fig. 3). This is apparent in all three oceanic reanalyses and the two SST analyses products. It may be noted that higher isotherms beyond the 29 °C isotherm were not included as the sample size reduces considerably, with a number of years not being able to reach 29 °C in the region during the ASO season.

3.2 Surface evolution of the AWP

Figure 4 shows the lagged (AWP lagging) correlations of the AWP with global SST in the three oceanic reanalyses while Fig. 5 shows the same relationship in the two SST

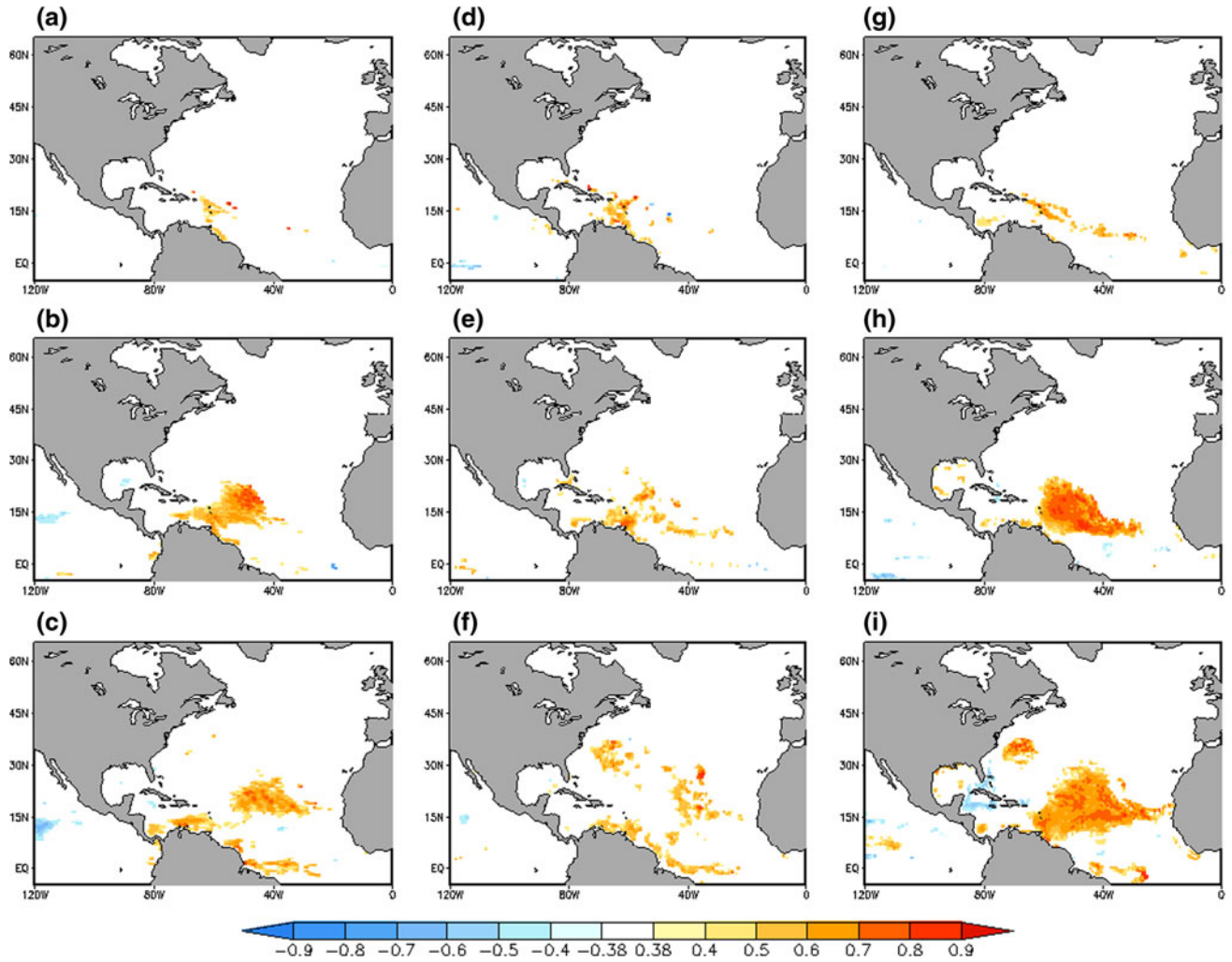

Fig. 6 The correlations of ASO averaged AWP area with the depth of the 26 °C isotherm **a** at two season lag (with AWP area lagging i.e., with preceding FMA 26 °C depth anomalies), **b** at one season lag (i.e., with preceding MJJ 26 °C depth anomalies), and **c** at zero lag (i.e., with contemporaneous ASO 26 °C depth anomalies) from GODAS. **d**, **e**, and **f** similar to **a**, **b**, and **c** but from SODA. **g**, **h**, and **i** similar to **a**, **b**, and **c** but from CFSR. Only statistically significant correlations at 95 % confidence interval according to *t* test are shown

analyses. A striking similarity across all three oceanic reanalyses (Fig. 4) that is consistent with the SST analyses (Fig. 5) is the pre-conditioning role of the tropical and subtropical Atlantic SST anomalies almost two seasons in advance. Another apparent resemblance across the reanalyses (Fig. 4) and SST analyses (Fig. 5) is the relative independence of the AWP interannual variations from the tropical Pacific variations. However, there are some significant differences in the association of the AWP evolution with the tropical Indian Ocean variability. The AWP in CFSR (GODAS) shows the weakest (strongest) association with the tropical Indian Ocean (Fig. 4). Both the SST analyses (Fig. 5), however, show consistently a strong positive correlation at two, one and zero season lags over the tropical Indian and western Pacific Ocean. Penland and Matrsova (2008) in their observational study allude to this teleconnection between the tropical Atlantic and the western Indian Ocean to the propagation of Rossby waves arising from convection in the latter region.

3.3 Subsurface evolution of the AWP

The subsurface evolution of the surface manifestation of the AWP is shown in Fig. 6. Here we show the lagged correlations at two, one, and zero season lags of the depth of the 26 °C isotherm with the area of the AWP. The local intrinsic to tropical Atlantic subsurface manifestation of the AWP variations is apparent from about one season lag in all three reanalyses (Fig. 6b, e, h). However, SODA (CFSR) shows the weakest (strongest) link of AWP with the 26 °C depth anomalies. The intriguing feature with GODAS is that the AWP correlation with the depth of the 26 °C isotherm diminishes in magnitude and spatial extent from one season to zero lag. It may be noted that as we go

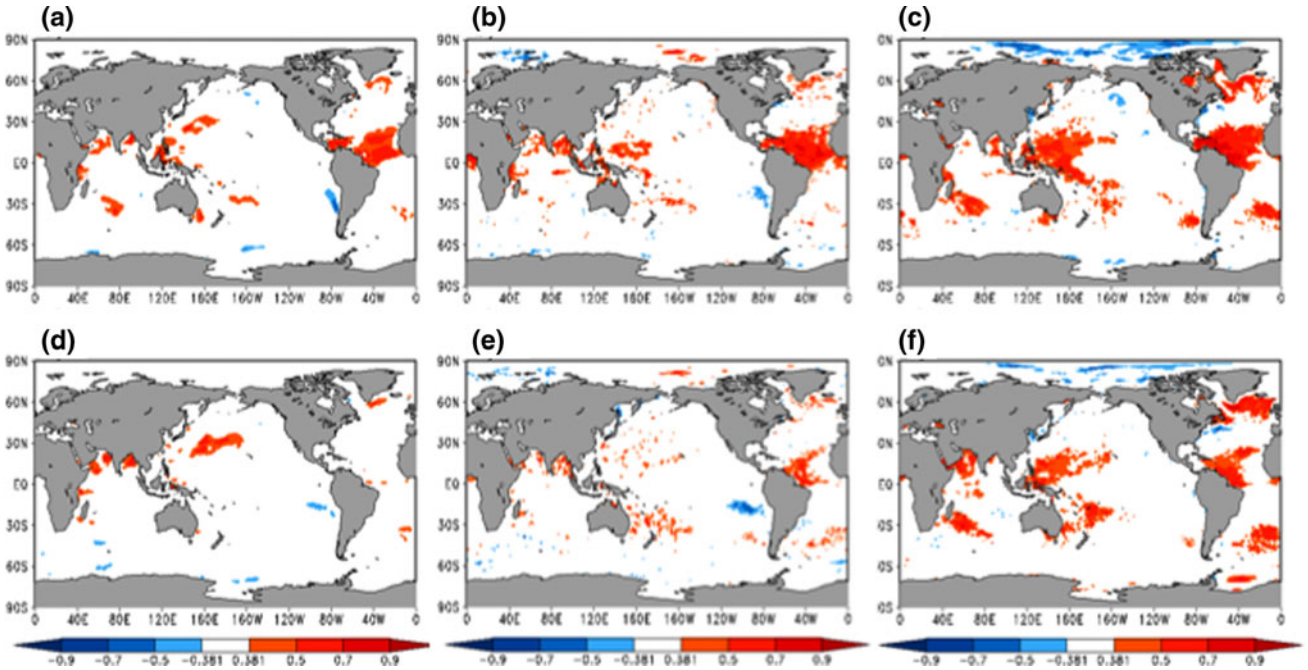

Fig. 7 The correlation of ASO averaged AWP area with succeeding November–December–January (NDJ) global SSTA from **a** GODAS, **b** SODA, and **c** CFSR. Similarly, correlation of ASO averaged AWP area with succeeding February–March–April (FMA) global SSTA from **d** GODAS, **e** SODA, and **f** CFSR. Only statistically significant values at 95 % confidence interval according to *t* test are shown

to depths of cooler isotherms (e.g. 20 °C isotherm) the correlations become insignificant (not shown). The positive correlations at one and zero season lags in Fig. 6 appear in a smaller region than in the corresponding lags in SST (Fig. 4), which suggests that overlying atmospheric influence alongside subsurface oceanic influence are both possibly playing critical roles in the variability of the AWP.

3.4 Demise of the AWP

The correlation of the variations of area of AWP with the following season SST (November–December–January [NDJ]) is largely confined to the tropical Atlantic in GODAS (Fig. 7a) and SODA (Fig. 7b) with the exception of CFSR (Fig. 7c) that shows strong positive correlations in tropical western Pacific Ocean as displayed by the SST analyses (Fig. 8). However, CFSR clearly does not represent the teleconnection of the mean ASO AWP variability with the tropical Indian Ocean in the subsequent NDJ season unlike in the SST analyses. The withdrawal of correlations in the Gulf of Mexico and western subtropical Atlantic Ocean from ASO (Figs. 4c, f, i, 5c, f) to NDJ (Figs. 7a–c, 8a, c) is also quite apparent and consistent in the reanalyses and SST analyses. At two season lags from ASO (i.e., February–March–April [FMA] season) the three reanalyses display further shrinking of the area with significant correlations in the tropical Atlantic (Fig. 7d–f), which is quite contrary to the corresponding figures from the two SST analyses (Fig. 8b, d). In other words, the memory of the surface ocean to AWP variations is relatively short in the three oceanic reanalyses compared to the two SST analyses.

Likewise the demise of the AWP in the subsurface ocean is more abrupt than its evolution (Fig. 9). In the case of GODAS, in just one season lead (Fig. 9a) the correlations of AWP variations with the depth of the 26 °C isotherm disappears completely from some positive correlations at zero lag (Fig. 6c) and one season lag (Fig. 6b). It is not surprising that SODA, which already displayed a weak relationship of the AWP variability with the subsurface ocean temperatures, (Fig. 6d–f) does not show any significant correlations at one (Fig. 9b) and two (Fig. 9e) season leads. In Fig. 9c, CFSR shows a diminishing relationship between the AWP variability and the depth of the 26 °C isotherm, which becomes nearly insignificant by two season lead (Fig. 9f).

3.5 Atmospheric response to the AWP

The tropical tropospheric temperature warming during warm ENSO episodes highlighted in many studies (Yulaeva and Wallace 1994; Horel and Wallace 1981; Chiang and Sobel 2002) is one of the many noticeable atmospheric responses to warming in the eastern equatorial Pacific Ocean. Sobel et al. (2002) showed that the Niño3 SST anomalies lead the tropospheric temperature anomalies

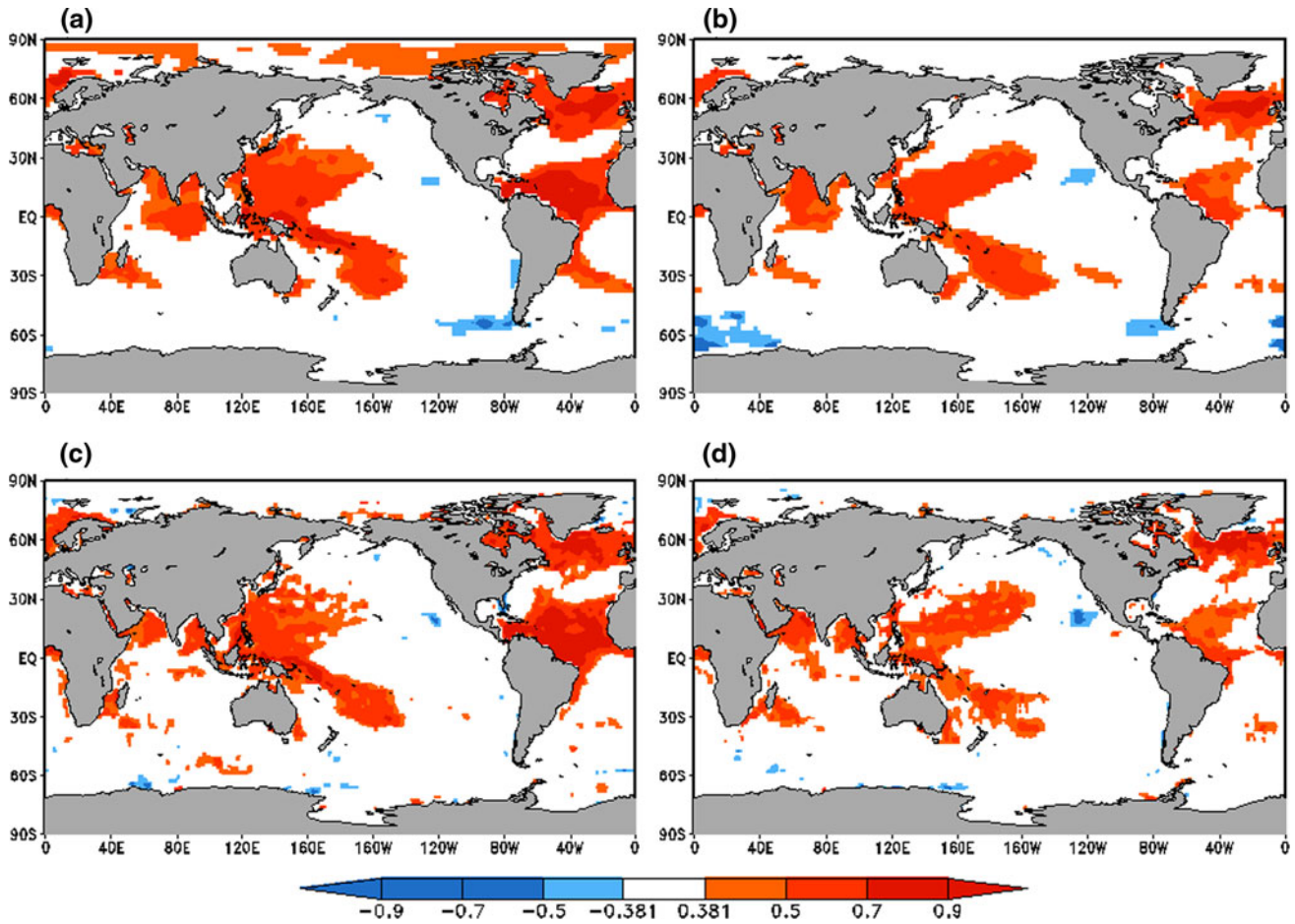

Fig. 8 The correlation of ASO averaged AWP area with **a** succeeding November–December–January (NDJ) and **b** succeeding February–March–April (FMA) global SSTA from ERSSTv3. Similarly the correlation of ASO averaged AWP area with **a** succeeding November–December–January (NDJ) and **b** succeeding February–March–April (FMA) global SSTA from OISSTv2. Only statistically significant values at 95 % confidence interval according to *t* test are shown

(computed as a pressure weighted average between 850 and 200 hPa) by as much as 8–10 months. In a similar vein, Lee et al. (2008) using idealized modeling studies showed that convection from AWP variations also generates a Gill type atmospheric response. In Fig. 10 we show the correlations of the tropospheric temperature anomalies with AWP variations at zero and one season lead (following NDJ season). At zero season lag, GODAS-R2 (Fig. 10a) and CFSR (Fig. 10c) display similar correlation patterns with widespread correlations from the AWP region to the east up to the tropical western Pacific Ocean. There is a clear absence of the influence of the AWP variations over the eastern tropical Pacific in all three atmospheric reanalysis. SODA-R1 displays the weakest atmospheric response with near absence of significant positive correlations over the tropical Indian Ocean. By one season lag (following NDJ season) all three reanalyses lose the spatial coherency of the correlations with the positive correlations appearing sporadically scattered in the global tropics (Fig. 10d–f). However, at a one season lag there are subtle differences between the reanalyses, with CFSR uniquely extending the correlation with the tropospheric temperature anomalies in the southern Indian and Atlantic Oceans and persisting with the correlations in the tropical eastern Atlantic Ocean (Fig. 10f).

3.6 Analysis of the SST in the AWP region

In this sub-section we examine the approximate SST anomaly equation (Eq. 1) given below, following Kang et al. (2001) and Misra (2008).

$$\frac{\partial T'}{\partial t} = -u_M \frac{\partial T'}{\partial x} - v_M \frac{\partial T'}{\partial y} - u' \frac{\partial T}{\partial x} - v' \frac{\partial T}{\partial x} - w_M \frac{\partial T'}{\partial z} - [w - w_M] \frac{\partial T}{\partial z} - H' \quad (1)$$

where T' is the SSTA, u_M and v_M are climatological zonal and meridional currents, w_M is the climatological vertical

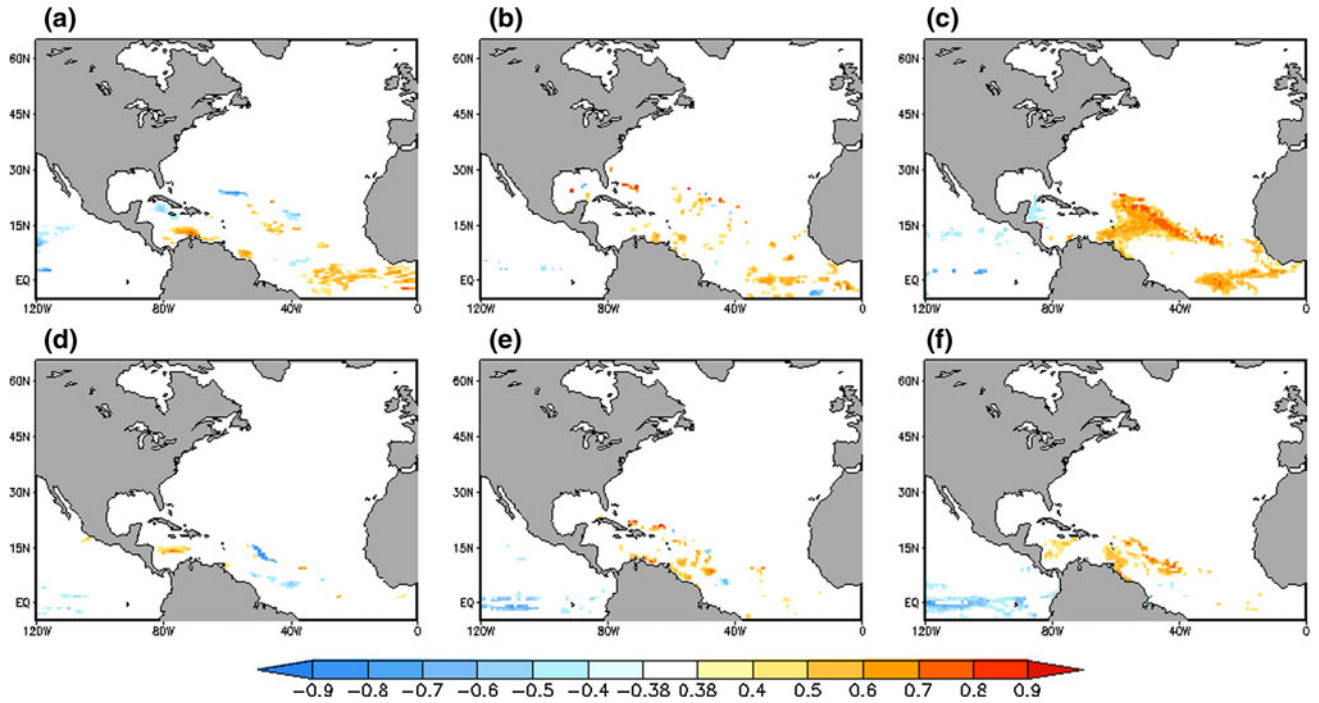

Fig. 9 Same as Fig. 7 but showing correlations of ASO averaged AWP area with 26 °C depth anomalies

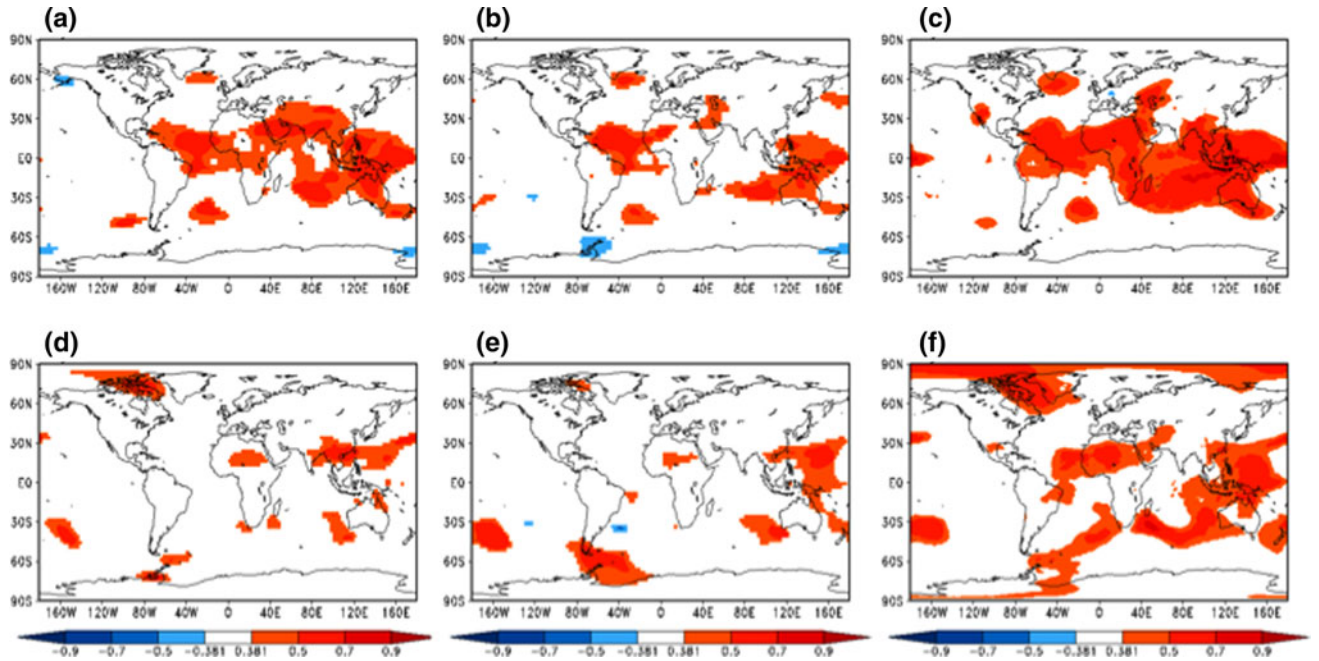

Fig. 10 The correlations of the mean ASO AWP with tropospheric temperature anomalies at **a** zero season lag (ASO season), **d** one season lead (tropospheric temperature anomalies from following NDJ season) obtained using GODAS SST and R2 tropospheric temperature. **b**, **e** Similar to **a** and **d** but using SST from SODA and tropospheric temperature from R1. **c**, **f** Similar to **a** and **d** but using SST and tropospheric temperature from CFSR

velocity, and H′ is the residual term of the atmospheric fluxes and dissipation. We have adapted here the SST anomaly equation originally developed to diagnose the ENSO variability for examination of the AWP variations. As suggested in the previous studies, the aim here is not to compute the SST budget but to understand the relative importance of the various terms in the SST anomaly equation. Towards this end we compute a "standardized

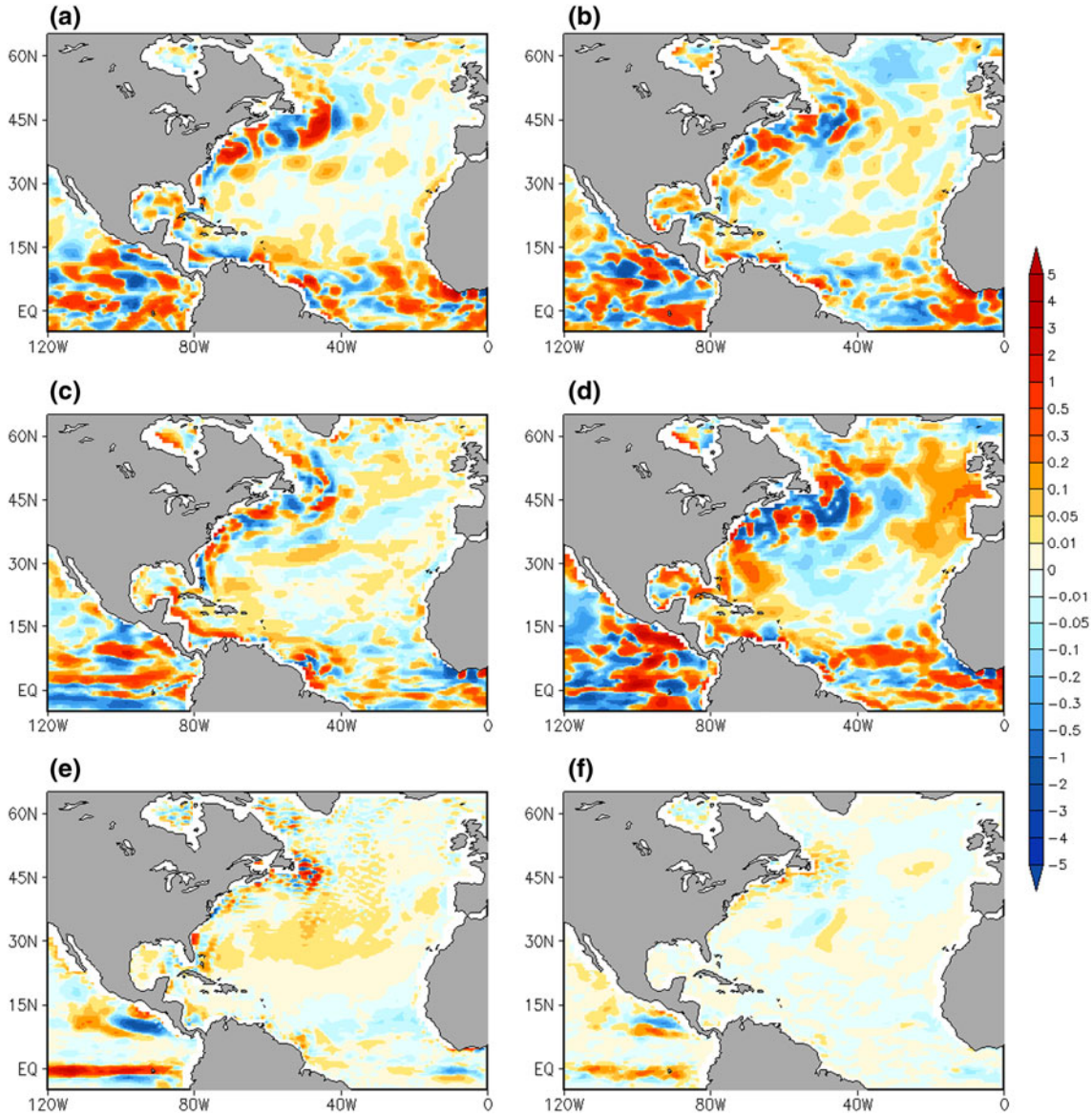

Fig. 11 The standardized covariance (see text for definition) of the SST tendency averaged over the AWP area in ASO season with contemporaneous values of the dynamic terms in the SST tendency equation **a** $-u_m \frac{\partial T'}{\partial x}$, **b** $-u' \frac{\partial T}{\partial x}$, **c** $-v_m \frac{\partial T'}{\partial y}$, **d** $-v' \frac{\partial T}{\partial y}$, **e** $-w_m \frac{\partial T'}{\partial z}$, and **f** $-w' \frac{\partial T}{\partial z}$ from GODAS. The units are in °C month^{-1}

covariance" (SCOV), which is the covariance of each of the terms on the right hand side of Eq. 1 with the time tendency of the SST averaged over the AWP region, that is divided by the standard deviation of the time tendency of the SST averaged over the AWP region. To compute SCOV, following Kang et al. (2001) we have averaged the terms on the right hand side of Eq. 1 from the surface to 50 m depth to represent the variations of the mixed layer of the ocean. Mathematically,

$$SCOV = \frac{\sum_{i=1}^{N} (x_i - \bar{x})(y_i - \bar{y})}{\sigma_x} \quad (2)$$

where x_i is the time tendency of the SSTA averaged over the AWP region and y is the individual forcing term on the right hand side of Eq. 1, and σ_x represents the standard deviation of the time tendency of the SST averaged over the AWP region. In this way SCOV will signify the actual magnitude of y that is related to the time series of the tendency of the SST anomalies over the AWP. Figure 11 shows the SCOV with the advective (or dynamic) terms of Eq. 1 from GODAS. Figure 11a–d are related to the advection of the anomalous and total temperature by the mean and anomalous horizontal currents. The standardized covariances are relatively noisy in these panels and identify very closely with some of the well-known surface currents in the region (e.g., Caribbean, Yucatan, Gulf stream, Florida, North Brazil, and North equatorial currents). The vertical advection by the mean upwelling of the anomalous

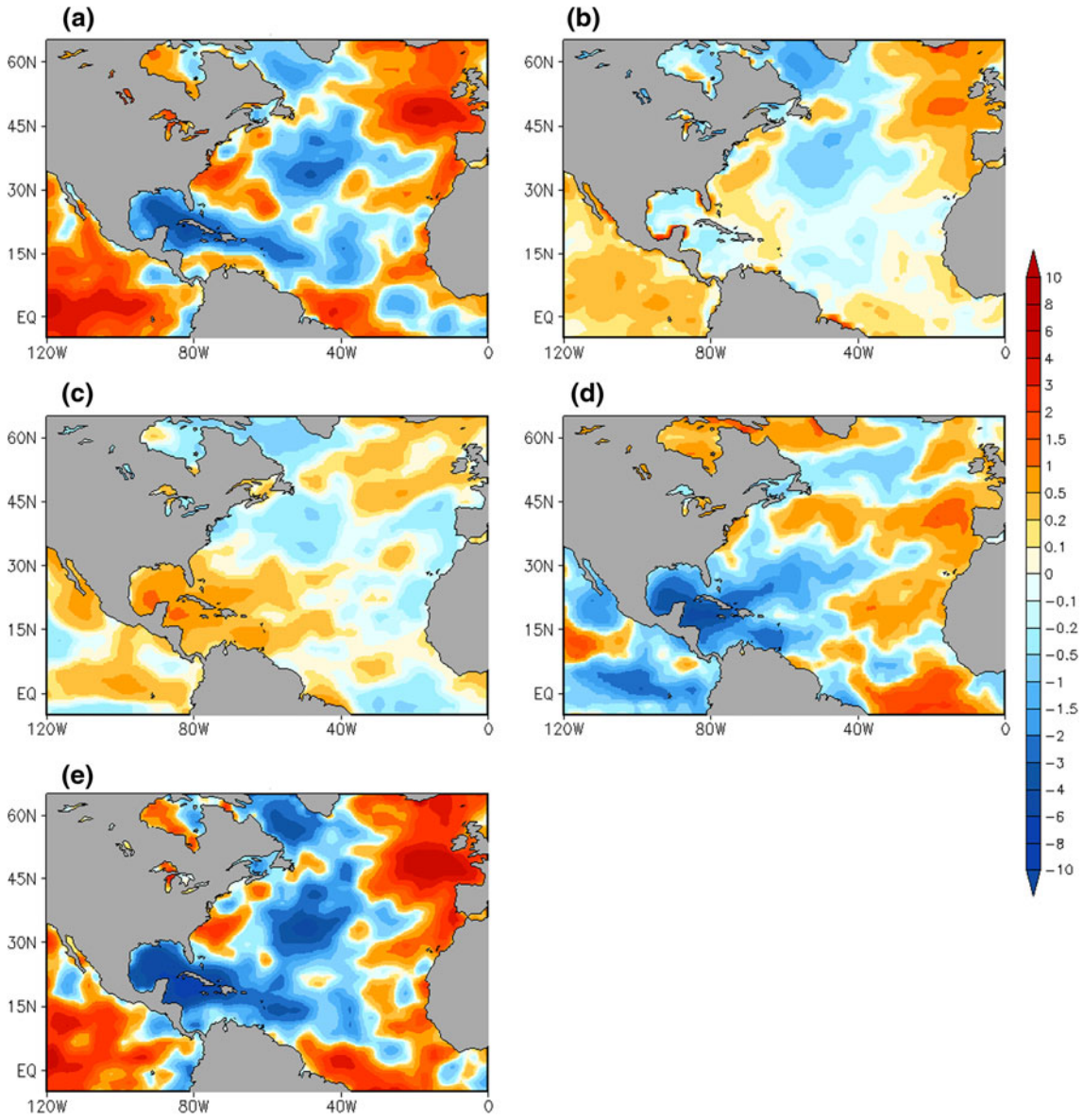

Fig. 12 Same as Fig. 11 but standardized covariance of the SST tendency averaged over the AWP area in the ASO season with **a** net heat flux, **b** latent heat flux, **c** sensible heat flux, **d** net long wave flux, and **e** net shortwave flux at surface from GODAS. The fluxes are obtained from the forcing fields of GODAS, which is the NCEP-DOE reanalysis (R2)

temperature has a coherent pattern in the subtropical Atlantic, remote to the AWP region (Fig. 11e). The advection of the anomalous upwelling of the total temperature is relatively weak (Fig. 11f). In summary, the impact of the dynamic terms on the evolution of the AWP is relatively weak but possibly subtle. Clement et al. (2005) indicate that ocean dynamics play an essential role in the maintenance of the warm pools. The other two reanalyses showed similar magnitude and patterns of SCOV for the dynamic terms (not shown).

In Fig. 12a we show the SCOV with the net heat flux from GODAS-R2 reanalysis. In computing this term, we took the net heat flux to be positive when it was upward from ocean to the atmosphere. So a negative SCOV in the AWP region in Fig. 12a would suggest that a reduction in the tendency of the SSTA is associated with a net increase in the heat flux coming out of the ocean. It may be noted that this SCOV is relatively far more spatially coherent in the AWP region and has a much larger magnitude than any of the dynamic terms shown in Fig. 11. In examining through the components of the net heat flux, the contribution of the latent heat flux (LHF; Fig. 12b), sensible heat flux (SHF; Fig. 12c), shortwave flux (SWF; Fig. 12d), and long wave flux (LWF; Fig. 12e) to the time tendency of the

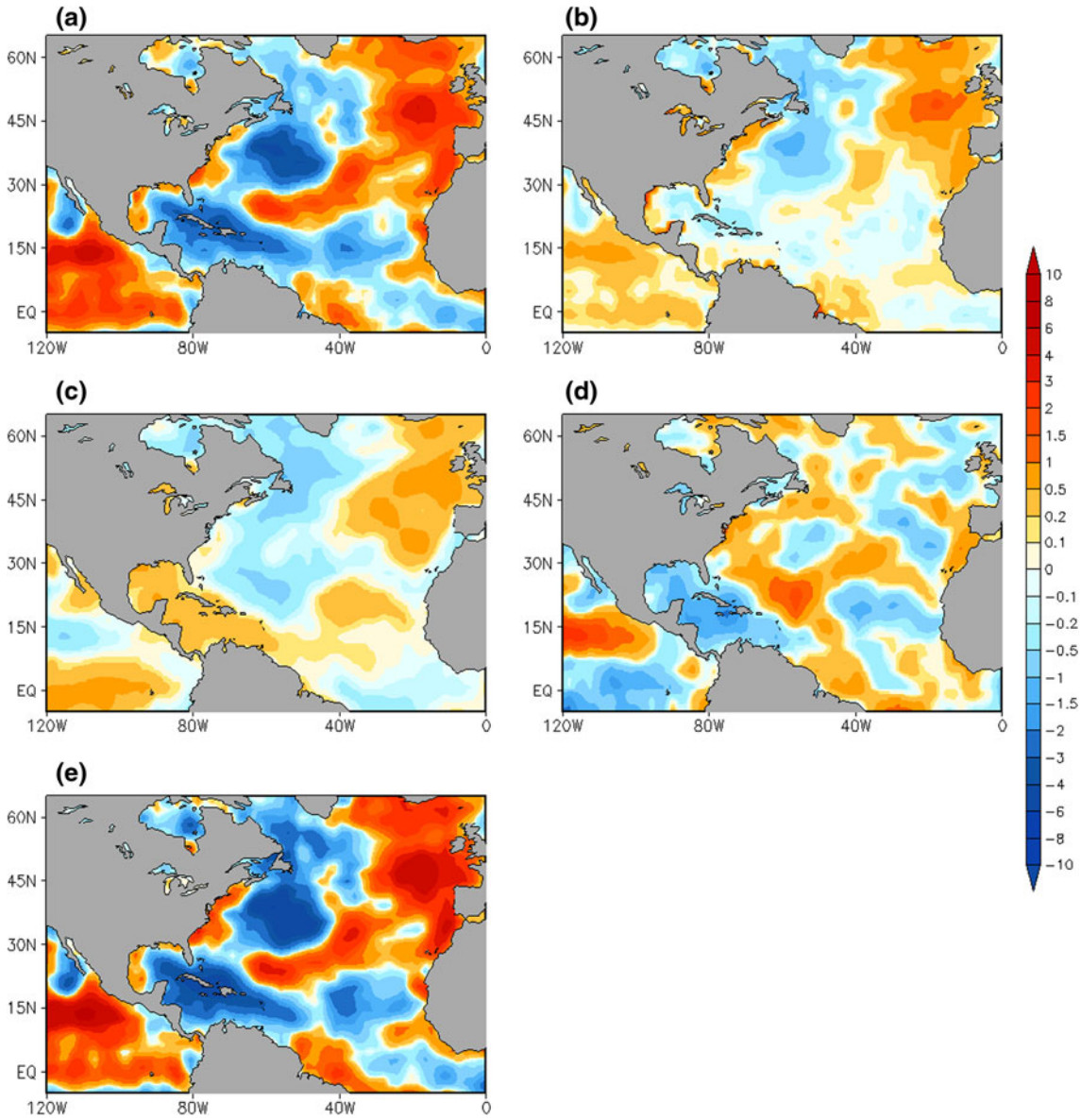

Fig. 13 Same as Fig. 11 but standardized covariance of the SST tendency averaged over the climatological AWP area for ASO with **a** net heat flux, **b** latent heat flux, **c** sensible heat flux, **d** net long wave flux, and **e** net shortwave flux at surface from SODA. The fluxes are obtained from the forcing fields of SODA, which is the NCEP-NCAR reanalysis (R1)

SST anomalies, it is seen that LHF has the weakest influence and SHF forcing tends to damp the influence of the radiative fluxes. However, it is apparent that the influence of the net heat flux on the tendency of the SST anomalies in GODAS is dominated by the variations of the LWF and SWF in R2 reanalysis in the AWP region. Similarly, SODA-R1 (Fig. 13) and CFSR (Fig. 14) indicate that the tendency of SSTA in the AWP region is dominated by variations of the net heat flux (Figs. 13a, 14a), which in turn are dictated largely by the variations of SWF (Figs. 13d, 14d) and LWF (Figs. 13e, 14e). It may, however, be noted that Wang et al. (2010) indicate that CFSR overestimates the downward solar radiation flux over the tropical western hemisphere warm pool associated with a positive SST bias.

We also examined the correlation of the time tendency of the SSTA averaged over the climatological AWP with rainfall (Fig. 15) and total cloud cover (Fig. 16). Despite the issue of fidelity of rainfall and total cloud cover in the reanalyses, both Figs. 15 and 16 show a consistency in the correlations with the tendency of SSTA in the AWP (especially over the Gulf of Mexico and western Caribbean Sea) increasing with reduced rainfall and total cloud cover. This is also consistent with the fact that both increased

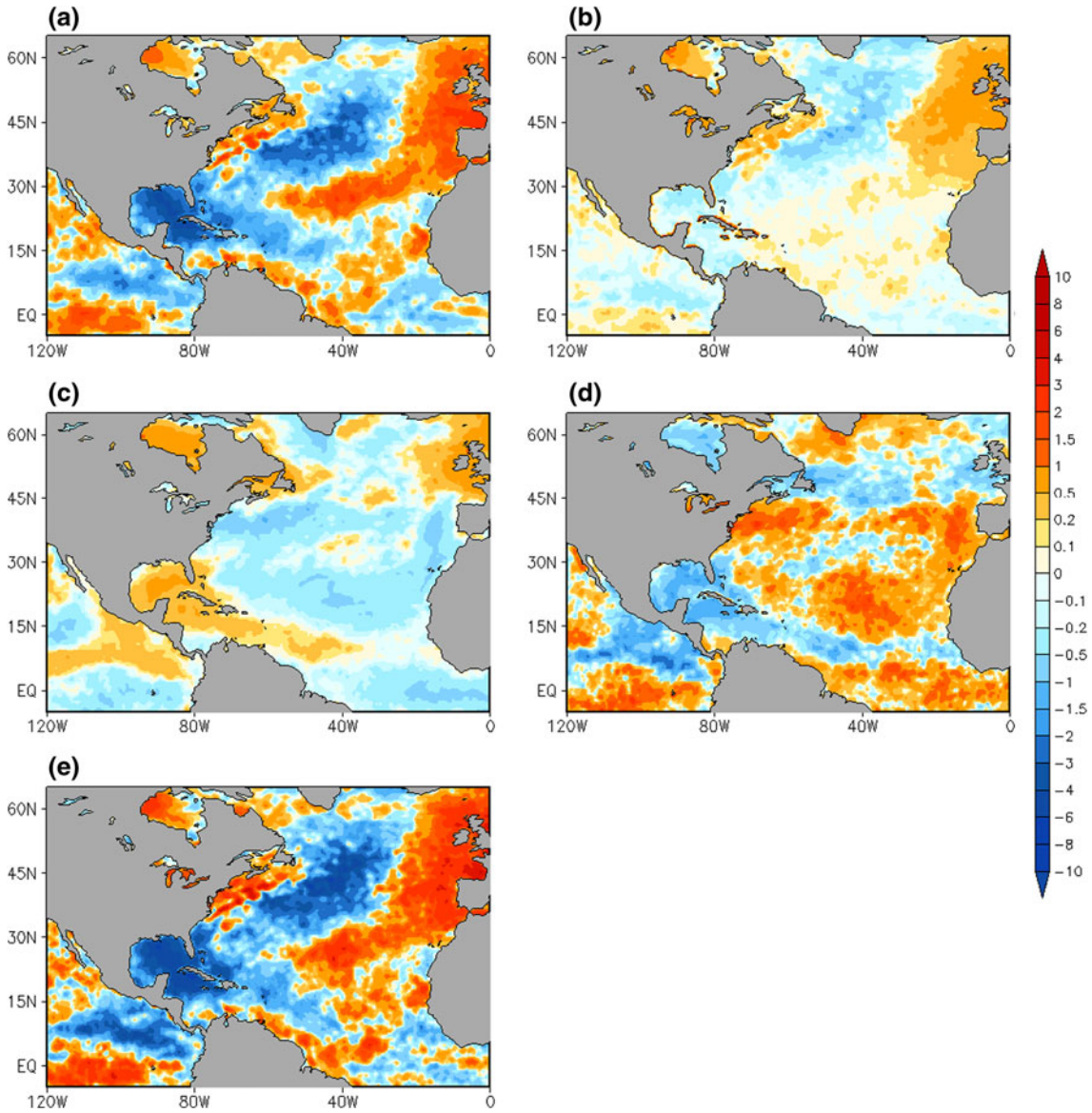

Fig. 14 Same as Fig. 11 but standardized covariance of the SST tendency averaged over the climatological AWP area for ASO season with **a** net heat flux, **b** latent heat flux, **c** sensible heat flux, **d** net long wave flux, and **e** net shortwave flux at surface from GODAS. The fluxes are obtained from the forcing fields of CFSR, which is CFSR atmosphere itself

downwelling shortwave flux and reduced upwelling long wave flux, which are usually associated with reduced cloud cover and rainfall are dominating influences on the changes in SST over the AWP region. Furthermore Fig. 17 shows that in this region of the AWP (i.e., Gulf of Mexico and western Caribbean Sea) the mean sea level pressure anomaly rises [more appreciably in R2 (Fig. 17a) and CFSR (Fig. 17c) compared to R1 (Fig. 17b)] with the increase in SST tendency over AWP. However, Fig. 17 also shows that the Bermuda high weakens in the subtropical latitudes and mean sea level pressure anomaly rises in the northern latitudes with the rise in SST tendency over AWP.

4 Summary and conclusions

The AWP is increasingly being recognized as one of the main drivers of boreal summer and fall seasonal climate variations in the western hemisphere. However, the AWP is one of the most poorly observed oceanic regions of our planet, which is unlike the observational network instituted to monitor ENSO variations in the tropical Pacific Ocean. In light of this fact, our study is an attempt to compare a modest number of reanalyses products for their rendition of the AWP. Although a broad and coarse conclusion could be made that AWP is relatively similar

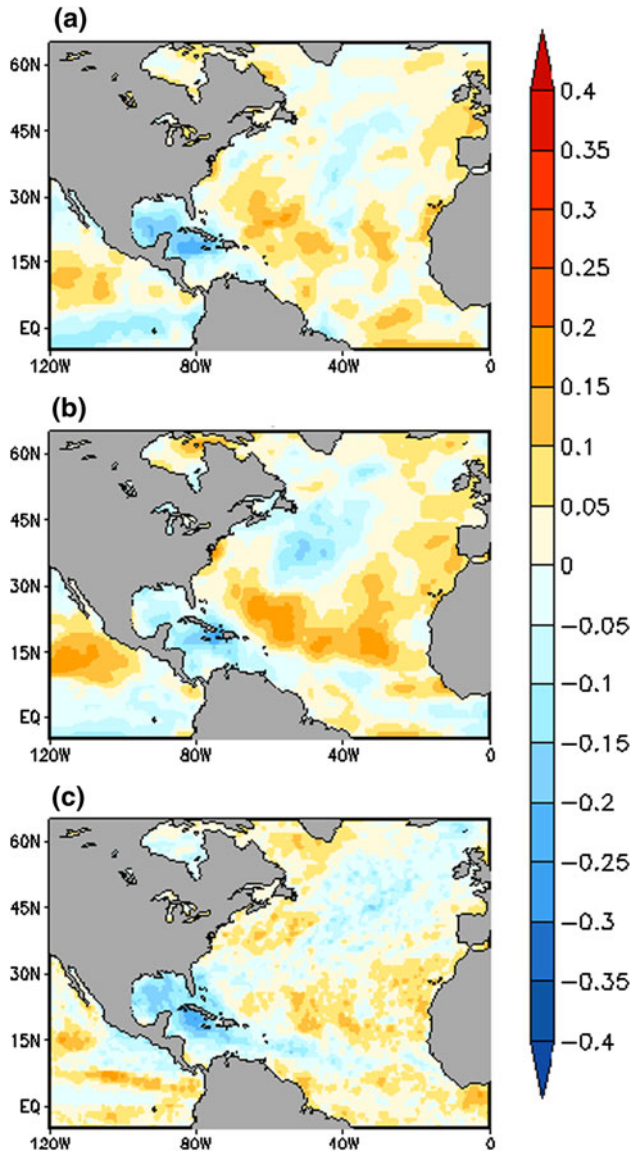

Fig. 15 Correlation of the SST tendency averaged over the climatological AWP area in the ASO season with corresponding rainfall. **a** SST tendency is computed from GODAS and rainfall is from R2, **b** SST tendency is computed from SODA and rainfall is from R1, **c** SST tendency and rainfall are from CFSR

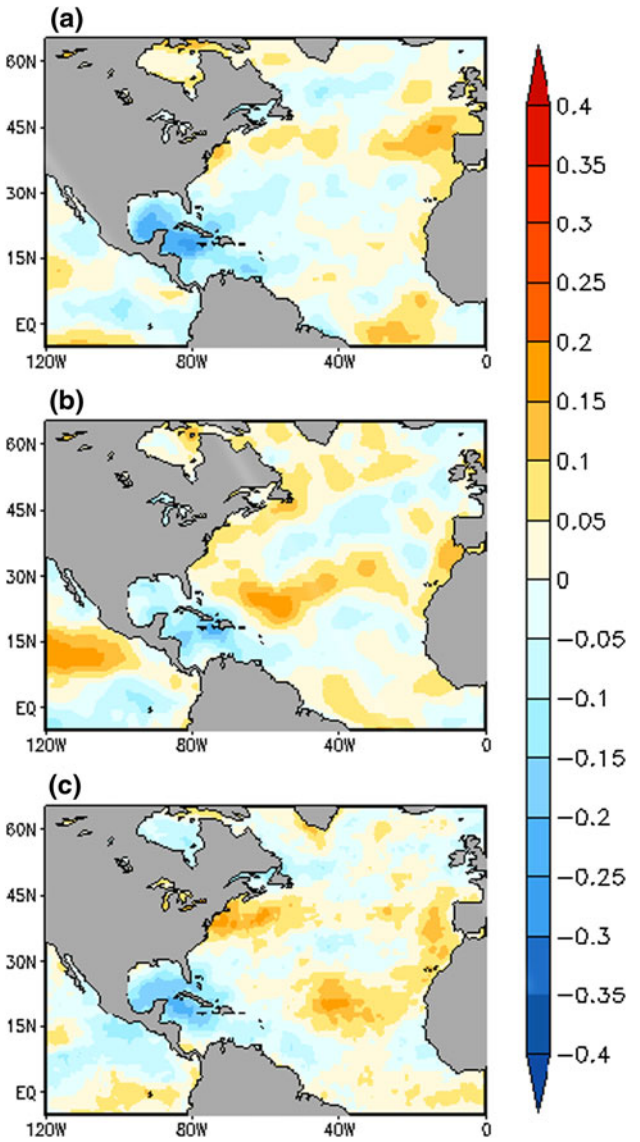

Fig. 16 Same as Fig. 15 but the correlation is between SST tendency averaged over the climatological AWP area in ASO season with cloud cover

across the reanalyses, it belies the subtle but important differences and limitations of the datasets. The comparisons of the datasets show:

1. There is a significant difference in the climatological area of the AWP across the three oceanic reanalyses. They systematically underestimate the area at the seasonal peak of AWP relative to the two SST analyses. The seasonal cycle of the AWP is, however, consistent in all three oceanic reanalyses and the two SST analyses.
2. The interannual variations of the SST in the AWP region show considerable differences with GODAS showing the least variability of the three oceanic reanalyses. However, all three oceanic reanalyses underestimate the interannual variability with respect to the two SST analyses.
3. The remote surface manifestation of the AWP, as expressed by the lag-lead relationship with SST, show considerable discrepancy across the three reanalyses, with the remote teleconnection over the Indian Ocean and western Pacific Ocean being inconsistently depicted across the reanalyses. The demise of the AWP in the subsequent NDJ season shows inconsistent modulation of the tropical Atlantic SST anomalies across the three reanalyses as well.

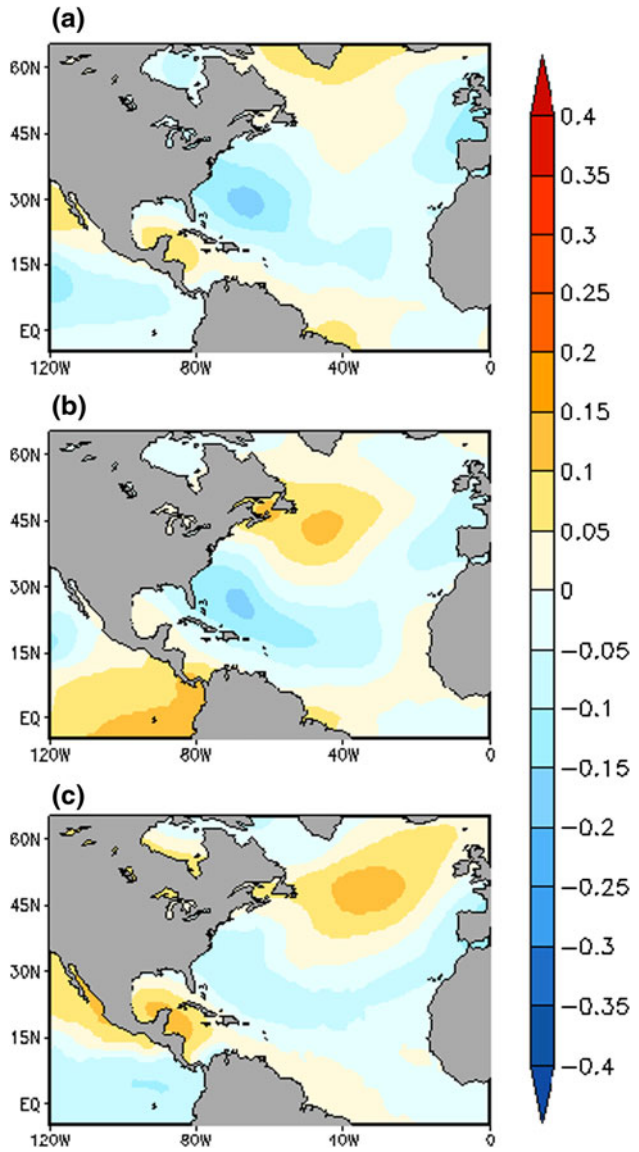

Fig. 17 Same as Fig. 15 but the correlation is between SST tendency averaged over the climatological AWP area in ASO season with mean sea level pressure

4. The subsurface evolution and subsequent demise of the AWP is even more contentious. For example, SODA shows very weak relationship with local upper ocean heat content compared to CFSR. The demise of the AWP, especially in terms of upper heat content anomalies (depth anomalies of the 26 °C isotherm), is relatively more abrupt in SODA. In CFSR, the demise is depicted more gradually.
5. The response of the tropospheric temperature anomalies to the AWP also shows subtle differences with the most widespread response in the global tropics displayed by CFSR, whereas, the anomalies of the tropospheric temperature anomalies are least widespread in R1. However, all three atmospheric reanalyses (R1, R2, and CFSR) do not show any response of the tropospheric temperature anomalies over the tropical eastern Pacific and do show a significant weakening of the tropospheric temperature anomalies by the subsequent NDJ season.
6. Our analysis shows that the variability of the AWP is dominated by the variability of the net heat flux. While the oceanic advective terms are relatively small, we recognize that they are quite likely playing an important role in the maintenance of the warm pool (Clement et al. 2005). We further show in this study that the variability of the radiative flux terms dominate the net heat flux term with the variations of the latent heat flux being comparatively the smallest. The co-variability of rainfall, total cloud cover and mean sea level pressure with the SST tendency in the AWP region further reaffirm the important role of cloud-radiative feedbacks in regulating the SST in the AWP region.

Acknowledgments This research was supported by NOAA grant NA09OAR4310170, USGS grant G10AC00149 and CDC grant U01EH000421.

References

Behringer D, Xue Y (2004) Evaluation of the global ocean data assimilation system at NCEP: the Pacific Ocean. Eighth symposium on integrated observing and assimilation systems for atmosphere, oceans, and land surface, AMS 84th annual meeting, Washington State Convention and Trade Center, Seattle, Washington, 11–15 Jan

Breigleb BP, Minnis P, Ramanathan V, Harrison E (1996) Comparison of radiational clear-sky albedos inferred from satellite observations and model computations. J Clim Appl Meteor 25:214–226

Campana KA, Hou Y-T, Mitchell KE, Yang S-K, Cullather R (1994) Improved diagnostic cloud parameterization in NMC's global model. In: Preprints, 10th Conf. on numerical weather prediction, Portland, OR, Am. Meteor. Soc., pp 324–325

Carton JA, Giese BS (2008) A reanalysis of ocean climate using simple ocean data assimilation (SODA). Mon Weather Rev 136:2999–3017

Carton JA, Chepurin G, Cao X (2000a) A simple ocean data assimilation analysis of the global upper ocean 1950–1995. Part 1: methodology. J Phys Ocean 30:294–309

Carton JA, Chepurin G, Cao X (2000b) A simple ocean data assimilation analysis of the global upper ocean 1950–1995. PartII: results. J Phys Ocean 30:311–326

Chiang JCH, Sobel AH (2002) Tropical tropospheric temperature variations caused by ENSO and their influence on the remote tropical climate. J Clim 15:2616–2631

Chou M-D (1992) A solar radiation model for use in climate studies. J Atmos Sci 49:762–772

Chou M-D, Lee K-T (1996) Parameterization for the absorption of solar radiation by water vapor and ozone. J Atmos Sci 53:1203–1208

Clement AC, Seager R, Murtugudde R (2005) Why are there tropical warm pools? J Clim 18:5294–5311

Conkright ME, Levitus S, O'Brien T, Boyer TP, Stephens C, Johnson D, Baranoca O, Antonov J, Gelfield R, Rochester J, Forgy C (1999) World ocean database 1998, documentation and quality control version 2.0, national oceanographic data center internal report 14, national oceanographic data center, Silver Spring, MD

Derber JC, Parris DF, Lord SJ (1991) The new global operational analysis system at the National Meteorological Center. Mon Weather Rev 6:538–547

Enfield DB, Mayer DA (1997) Tropical Atlantic sea surface temperature variability and its relation to El Niño-Southern Oscillation. J Geophys Res 102:929–945

Higgins W, Shi W (2001) Intercomparison of the principal modes of interannual and intraseasonal variability of the North American monsoon system. J Clim 14:403–417

Horel JD, Wallace JM (1981) Planetary-scale atmospheric phenomena associated with the Southern oscillation. Mon Weather Rev 109:813–829

Kalnay E et al (1996) The NMC/NCAR 40-year reanalysis project. Bull Am Soc 77:437–471

Kanamitsu M, Ebisuzaki W, Woollen J, Yang S-K, Fiorino JJ, Potter GL (2002) NCEP-DOE AMIP-II reanalysis (R-2). Bull Am Soc 83:1631–1643

Kang I-S, An I-S, Jin F–F (2001) A systematic approximation of the sst anomaly equation for enso. J Meteor Soc 79:1–10

Kleist DT, Parrish DF, Derber JC, Treadon R, Errico RM, Yang R (2009) Improving incremental balance in the GSI 3DVAR analysis system. Mon Weather Rev 137:1046–1060

Lee S-K, Wang C, Enfield D (2008) A simple atmospheric model of the local and teleconnection responses to tropical heating anomalies. J Clim 22:227–284

Maloney E, Hartmann D (2000) Modulation of the hurricane activity in the Gulf of Mexico by the Madden-Julian oscillation. Science 287:2002–2004

Misra V (2008) Coupled interactions of the monsoons. Geophys Res Lett 35:L12705. doi:10.1029/2008GL033562

Misra V (2009) Harvesting model uncertainty for simulation of interannual variability. J Geophys Res 114:D161113. doi:10.1029/2008JD011686

Misra V et al (2010) The IASCLiP modeling plan. Available from http://www.eol.ucar.edu/projects/iasclip/documentation/IASCLIP.Modelplan_latest.pdf

Pan H-L, Mahrt L (1987) Interaction between soil hydrology and boundary layer developments. Boundary-Layer Meterol 38:185–202

Parrish DF, Derber JC (1992) The national meteorological center's spectral statistical interpolation analysis system. Mon Weather Rev 120:1747–1763

Penland C, Matrsova L (2008) A southern hemisphere footprint in American Midwest precipitation. Geophys Res Lett L09703. doi:10.1029/2008GL033612

Reynolds RW, Rayner NA, Smith TM, Stokes DC, Wang W (2002) An improved in situ and satellite SST analysis for climate. J Clim 15:1609–1625

Saha S et al (2010) The NCEP climate forecast system reanalysis. Bull Am Soc. doi:10.1175/2010BAMS3001.1

Smith RD, Dukowicz JK, Malone RC (1992) Parallel ocean general circulation modeling. Physica D 60:38–61

Smith TM, Reynolds RW, Peterson TC, Lawrimore J (2008) Improvements to NOAA's historical merged land-ocean surface temperature analysis (1880–2006). J Clim 21:2283–2296

Sobel AH, Held IM, Bretherton CS (2002) The ENSO signal in tropical tropospheric temperature. J Clim 15:2702–2706

Tester PA, Feldman RL, Nau AW, Kibler SR, Litaker RW (2010) Ciguatera fish poisoning and sea surface temperatures in the Caribbean Sea and the West Indies. Toxicon. doi:10.1016/j.toxicon.2010.02.026

Wang C, Enfield DB (2001) The tropical western hemisphere warm pool. Geophys Res Lett 28:1635–1638

Wang C, Enfield D (2003) A further study of the tropical Western Hemisphere Warm Pool. J Clim 6:1476–1493

Wang C, Lee S-K (2007) Atlantic warm pool, Caribbean low-level jet, and their potential impact on Atlantic hurricanes. Geophys Res Lett 34. doi:10.1029/2006GL028579

Wang C, Enfield DB, Lee S-K, Landsea C (2006) Influences of the Atlantic warm pool on Western Hemisphere summer rainfall and Atlantic hurricanes. J Clim 19:3011–3028

Wang C, Lee S-K, Enfield DB (2008) Climate response to anomalously large and small Atlantic Warm pools during the summer. J Clim 21:2437–2450

Wang W, Xie P, Yoo S-H, Xue Y, Kumar A, Wu X (2010) An assessment of the surface climate in the NCEP climate forecast system reanalysis. Climate Dyn. doi:10.1007/s00382-010-0935-7

Yulaeva E, Wallace JM (1994) The signature of ENSO in global temperature and precipitation fields derived from the microwave sounding unit. J Clim 7:1719–1736

Zheng Y, Giese BS (2009) Ocean heat structure in simple ocean data assimilation: structure and mechanism. J Geophys Res 114. doi:10.1029/2008JC005190

Zheng Y, Shinoda T, Kiladis G, Lin J, Metzger EJ, Hurlburt HE, Geise BS (2010) Upper-Ocean processes under the stratus cloud deck in the southeaset Pacific Ocean. J Phys Oceanogr 40:103–120